 CMES, vol.3, no.6, pp.743-754, 2002

Computational Simulations of Micro-Indentation Tests Using Gradient Plasticity

Jian Chen[1], **Huang Yuan**[2] **and Folker H. Wittmann**[3]

Abstract: Experimental observation confirms that micro-hardness of metallic materials depends significantly on the indentation depth. In the present paper we discuss simulations of micro-indentation tests based on the gradient plasticity model using the finite element method. The role of intrinsic material length parameters in the gradient plasticity model is investigated. The computational results confirm that the gradient plasticity model is suitable to simulate micro-indentation tests and predicts the depth-dependent hardness in micro- and nano-indentations. Variations of micro-hardness is correlated with the intrinsic material length parameters.

keyword: Gradient-dependent plasticity, intrinsic material length, plastic strain gradients, size effects, micro-indentation, finite element method

1 Introduction

Increasing experimental evidence indicates that the plastic flow strength of materials depends on the absolute size of specimens, so-called size-effect. In torsion tests Fleck and Hutchinson (1993) found that the torque normalized by the twist of a thin wire of copper with a diameter of 12 microns was as high as three times of that of a wire with a diameter of 120 microns, whereas in uniaxial tension the material strength becomes scalable by the geometry factor. This observation implies that the material strength depends on strain gradients. In order to make an accurate prediction of structural integrity, it is important to know how the strain gradients affect strength of materials and how to quantify these effects.

Recently, experiments on micro- and nano-indentation hardness tests have been extensively adopted for determining material characteristics in micro-dimension [Ma, Clarke (1995); McEkhaney, Vlassak, Nix (1998); Poole, Ashby, Fleck (1996); Stelmashenko, et al. (1993)]. It has been found that the micro-hardness of materials is significantly higher than the macro-hardness by a factor of two or more in the range of the indentation depth from about 10 microns to 0.1 micron. Generally, it can be said the smaller the scale, the stronger will be the solid. Based on experimental observations Nix and Gao (1998) predict a linear relation of the square of the micro-hardness, H, and the inverse of the indentation depth, $1/h$, that is,

$$(\frac{H}{H_0})^2 = 1 + \frac{h^*}{h}, \tag{1}$$

where H_0 is the macro hardness and h^* is a material specific parameter depending on indenter angle as well as on the mechanical property of materials. Nix and Gao (1998) suggest $h^* = 3(\cos\beta)^2/(16b\rho_s)$, where b is the Burgers vector, ρ_s is the statistically stored dislocation density and β stands for half of the indenter's angle. The statistically stored dislocations are related to the plastic strain. In this way the micro-hardness is related to the indentation depth through the statistically stored dislocations ρ_s. It has been verified that equation (1) can be applied to predict the size effect of micro-hardness for many kinds of materials.

Conventional continuum mechanics assumes that the solid is homogeneous and does not contain heterogeneities. It follows that the stress state is determined by the deformation history of a material point itself. Although the conventional continuum mechanics is quite sufficient for many engineering applications, experimental evidences indicate that the inhomogeneity on the material micro-structure level may induce a strong depen-

[1] Current address: ALSTOM Power (Schweiz) AG, CH-5401 Baden, Switzerland
[2] Corresponding author. Tel.: +49-89-1489 9294; fax: +49-89-1489 2728; E-mail: huang.yuan@muc.mtu.de. Current address: MTU Aero Engines München, D-80995 Munich, Germany Lab. for Materials Behaviour, Paul Scherrer Institute, CH-5232 Villigen PSI, Switzerland
[3] Institute for Building Materials, ETH Zürich, CH-8093 Zürich-Hönggerberg, Switzerland

dence on the strength prediction and therefore the microstructure has to be considered in a suitable way in continuum models. A variety of methods which take effects of strain gradients into account has been proposed in recent years. Fleck and Hutchinson (1993), (1997) introduced the *strain gradient plasticity theory* in which additional strain quantities and the work conjugated couple stress quantities enter the continuum model. This strain gradient plasticity theory as well as its alternative form [Gao, Huang, Nix, Hutchinson (1999)] have been used to analyze the size effects of micro-indentation tests [Begley, Hutchinson (1998); Huang, et al. (2000); Shu, Fleck (1998)]. The strain gradient plasticity theory generates a new theoretical frame for continuum mechanics by introducing new field variables to meet the microstructural characteristics. One problem of such models is that the strain gradient effects in pure tension become small due to vanishing rotations and, furthermore, it is still an issue whether or not such models may predict a physical meaningful shear band result due to strain localizations. From the view point of finite element computations, effects of the introduced gradient regulators may be too weak to overcome the mesh-dependence in numerical analysis due to strain softening.

Aifantis (1987) suggested a simple form of plasticity model depending on plastic strain gradients which is termed the *gradient plasticity theory*. In his model Aifantis simply assumes that the actual flow stress is linearly related to the gradients of the equivalent plastic strain. The consistence of such gradient plasticity models has been discussed in the frame of thermodynamics by Valanis (1997) and Polizzotto, Borino (1998). In computational work by de Borst and his co-workers [deBorst, Mühlhaus (1992); Pamin (1994)] the flow stress is only related to the second order gradient (Laplacian) of the equivalent plastic strain. This model is successfully applied to failure analysis of concrete structures. It has been confirmed that the gradient plasticity provides a mesh-independent shear band for strain-softening materials. This formulation is extended to finite strain problems by Mikkelsen (1997) and Ramaswamy, Aravas (1998). A gradient plasticity theory coupled with damage mechanism is reported in [Chen, Yuan (2000); Sverberg, Runesson (1998)]. However, due to the analytical and computational difficulties [Yuan, Chen (2001)], most numerical efforts are limited in analysis of the shear band.

Recently, a modified *low-order gradient plasticity* model is proposed based on the Aifantis' gradient plasticity idea and Gao's flow stress formulation, in which the gradient of effective plastic strain $|\nabla\bar{\varepsilon}^p|$ is introduced into the flow stress, $\bar{\sigma} = \sigma_0\sqrt{f^2(\bar{\varepsilon}^p) + l|\nabla\bar{\varepsilon}^p|}$, with a material length parameter l. This model is used to analyze the size effect of ductile materials [Yuan, Chen (2000)] and provide results verified by known experimental observations. In micro-indentation simulation, the computational data of this model successfully fitted the correlation proposed by Nix and Gao (1998). However, the analysis of the strain-softening shear band is still open issue for this model.

According to the authors' knowledge, no results on the depth-dependent micro-indentation using high order gradients of plastic strains have been reported. The aim of the present paper is to investigate the effect of strain gradients in micro-indentation simulations. It is to be shown whether or not the phenomenological gradient plasticity model suggested by Aifantis (1987) can capture the depth-dependence of the micro-hardness correctly. Furthermore, we are going to examine the relationship between the micro-hardness and the indentation depth as observed with equation (1). In this sense the parameter h^* is used as a fitting parameter in the gradient plasticity model based on suitable assumptions. Finite element implementation of this gradient plasticity theory is used to analyze the size-dependent micro-hardness. The role of the first-order and the second-order derivatives of equivalent plastic strain is systematically investigated. Computational results confirm that the second-order gradient of equivalent plastic strain overestimates the hardness variation. The first-order gradient of plastic strain can be used to fit the known experimental prediction in [McElhaney, Vlassak, Nix (1998); Nix, Gao (1998)].

2 Computational gradient-dependent plasticity

The size effect of plastic flow strength is related to accumulations of dislocations generated by non-uniform straining. In plasticity the stress and strain state of a material point is influenced by distortions of its neighbor, i.e., plastic deformations are generally nonlocal. To consider the nonlocal effects in plasticity, the plastic strain gradient of a point should be introduced into a constitutive relationship under certain circumstances [Aifantis (1987)]. In this section we follow the framework of gradient plasticity and formulate the finite element equations. The model has been implemented into commercial finite element code ABAQUS using the user-element in-

terface [ABAQUS User Manual].

2.1 Governing equations

We assume that the uniaxial stress-strain relation can be described by a power-law hardening as

$$\overline{\sigma} = \sigma_0 \left(\frac{E\overline{\varepsilon}^p}{\sigma_0} \right)^N, \tag{2}$$

where E is Young's modulus, $N \leq 1$ is the plastic strain hardening exponent, σ_0 is the initial yield stress and $\overline{\varepsilon}^p$ is the equivalent plastic strain. In the frame of continuum mechanics the strain rate, $\dot{\varepsilon}_{ij}$, is related to the deformation velocity $\dot{u}_i$ by

$$\dot{\varepsilon}_{ij} = (\dot{u}_{j,i} + \dot{u}_{i,j})/2, \tag{3}$$

where the index comma in mathematical equations indicates the partial derivative in the spatial Cartesian coordinate system and a repeated suffix denotes summations over 1 to 3. It is assumed that the strain rate can be decomposed into elastic and plastic parts as following:

$$\dot{\varepsilon}_{ij} = \dot{\varepsilon}^{el}_{ij} + \dot{\varepsilon}^{pl}_{ij}. \tag{4}$$

The objective Jaumann stress rate according to plasticity theory can be expressed as

$$\sigma^{\nabla}_{ij} = C^e_{ijkl}\dot{\varepsilon}^{el}_{kl} \tag{5}$$

with the elasticity matrix C^e_{ijkl}. The choice of the Jaumann stress rate is by no means unique or even necessary according to the opion of Atluri (1984). It is, however, necessary to make use of ABAQUS interface in our work. For isotropic solids the elasticity matrix can be simplified into

$$C^e_{ijkl} = (K - \frac{2}{3}G)I_{ij}I_{kl} + 2GI'_{ijkl}, \tag{6}$$

where K and G are the elastic bulk and shear moduli, respectively. I_{ij} is the second order identity tensor, and I'_{ijkl} is the fourth order symmetric identity tensor with Cartesian components $I'_{ijkl} = (I_{ik}I_{jl} + I_{il}I_{jk})/2$. Substituting equation (4) into (5), it follows

$$\sigma^{\nabla}_{ij} = C^e_{ijkl}\dot{\varepsilon}_{kl} - C^e_{ijkl}n_{ij}\dot{\overline{\varepsilon}}^p. \tag{7}$$

In the equation above $n_{ij} = 2s_{ij}/3\overline{\sigma}$ denotes the plastic flow tensor, with s_{ij} as deviatoric stress tensor. The stress rate can be calculated from the Jaumann stress as

$$\dot{\sigma}_{ij} = \sigma^{\nabla}_{ij} + \sigma_{ik}\Omega_{kj} - \sigma_{jk}\Omega_{ik} \tag{8}$$

with $\Omega_{ij} = (\dot{u}_{i,j} - \dot{u}_{j,i})$ as the spin rate matrix due to finite rotation.

As suggested by Aifantis (1987), yield stress depends on both equivalent plastic strain and its gradients as

$$\sigma_y(\overline{\varepsilon}^p, |\nabla\overline{\varepsilon}^p|, \nabla^2\overline{\varepsilon}^p) = \overline{\sigma}(\overline{\varepsilon}^p) + g_1|\nabla\overline{\varepsilon}^p| - g_2\nabla^2\overline{\varepsilon}^p, \tag{9}$$

where $\sigma(\overline{\varepsilon}^p)$ denotes the yield stress expressed as a function of the equivalent plastic strain as in (2) and g_1, g_2 are positive coefficients. In this paper, g_1, g_2 are defined as:

$$g_1 = \sigma_0 c_1 f_1(\overline{\varepsilon}^p), \tag{10}$$

$$g_2 = \sigma_0 c_2^2 f_2(\overline{\varepsilon}^p), \tag{11}$$

where c_1 and c_2 are intrinsic material length scale parameters and f_1 as well as f_2 are dimensionless functions of equivalent plastic strain in general. Then the strain gradients were introduced into the constitutive equation by the flow stress and it follows

$$\Phi(\overline{\sigma}(\overline{\varepsilon}^p), |\nabla\overline{\varepsilon}^p|, \nabla^2\overline{\varepsilon}^p) = \phi(\overline{\sigma}(\overline{\varepsilon}^p)) + g_1|\nabla\overline{\varepsilon}^p| - g_2\nabla^2\overline{\varepsilon}^p, \tag{12}$$

where $\phi(\overline{\sigma}(\overline{\varepsilon}^p))$ is the classical J_2 yield condition. Should both g_1 and g_2 vanish, the gradient plasticity turns to classical J_2 plasticity.

The presence of the gradient terms in the constitutive equation needs additional boundary conditions for the equivalent plastic strain in the forms as

$$\delta(\dot{\overline{\varepsilon}}^p) = 0 \text{ or } \delta(\frac{\partial\dot{\overline{\varepsilon}}^p}{\partial\mathbf{v}}) = 0. \tag{13}$$

Equation (13) is assumed in [deBorst, Mühlhaus (1992); Mikkelsen (1997); Mülhaus, Aifantis (1991); Pamin (1994); Polizzotto, Borino (1998); Ramaswamy, Aravas (1998); Sverberg, Runesson (1998)], where $\mathbf{v}$ is the outwards normal vector. During plastic flow, the stress point must remain on the yield surface in the stress space

$$\dot{\Phi}(\sigma(\overline{\varepsilon}^p, |\nabla\overline{\varepsilon}^p|, \nabla^2\overline{\varepsilon}^p)) = 0, \tag{14}$$

which can be re-written as

$$\frac{\partial\Phi}{\partial\sigma_{ij}}\dot{\sigma}_{ij} + \frac{\partial\Phi}{\partial\overline{\varepsilon}^p}\dot{\overline{\varepsilon}}^p + \frac{\partial\Phi}{\partial|\nabla\overline{\varepsilon}^p|}|\nabla\dot{\overline{\varepsilon}}^p| + \frac{\partial\Phi}{\partial\nabla^2\overline{\varepsilon}^p}\nabla^2\dot{\overline{\varepsilon}}^p = 0. \tag{15}$$

For the von Mises plasticity, it is known that $\dot{\overline{\varepsilon}}^p = \lambda$ where λ is the plastic multiplier. Then the consistency condition takes the form as

$$n_{ij}\dot{\sigma}_{ij} + \frac{\partial\Phi}{\partial\lambda}\dot{\lambda} + \frac{\partial\Phi}{\partial|\nabla\lambda|}|\nabla\dot{\lambda}| + \frac{\partial\Phi}{\partial\nabla^2\lambda}\nabla^2\dot{\lambda} = 0. \tag{16}$$

with $n_{ij} = \partial\Phi/\partial\sigma_{ij}$. Let V and V^p denote the volume occupied by the body and the plastic part volume of the body, respectively. Let S be the surface bounding this volume and S^p be the so-called elastic-plastic boundary surface. Following the suggestion of Mülhaus and Aifantis (1991), de Borst and Mülhaus (1992), the generalized variational formulation can be expressed as

$$\Pi(u_i, \overline{\varepsilon}^p, \delta\dot{u}_i, \delta\dot{\lambda}) = \int_V (\sigma_{ij,j} + b_i)\delta\dot{u}_i \mathrm{d}V + \int_S \overline{t}_i\delta\dot{u}_i \mathrm{d}S$$
$$+ \int_{V^p} \Phi(\overline{\sigma}(\overline{\varepsilon}^p), |\nabla\dot{\overline{\varepsilon}}^p|, \nabla^2\overline{\varepsilon}^p)\delta\dot{\lambda}\mathrm{d}V + \int_{S^p} \frac{\partial\overline{\varepsilon}^p}{\partial\mathbf{v}}\delta\dot{\lambda}\mathrm{d}S. \tag{17}$$

The solution is obtained as soon as the generalized variational expression Π vanishes,

$$\Pi(u_i, \overline{\varepsilon}^p, \delta\dot{u}_i, \delta\dot{\lambda}) = 0. \tag{18}$$

To solve the above nonlinear integral equation, the Newton iteration method can be used. It follows two basic weak form equations as

$$\int_{V^p} \delta\dot{\lambda}(n_{ij}\dot{\sigma}_{ij} + \frac{\partial\Phi}{\partial\lambda}\dot{\lambda} + \frac{\partial\Phi}{\partial|\nabla\lambda|}|\nabla\dot{\lambda}| + \frac{\partial\Phi}{\partial\nabla^2\lambda}\nabla^2\dot{\lambda})\mathrm{d}V$$
$$= -\int_V \delta\dot{\lambda}\Phi^0(\sigma(\overline{\varepsilon}^p, |\nabla\overline{\varepsilon}^p|, \nabla^2\overline{\varepsilon}^p))\mathrm{d}V; \tag{19}$$

$$\int_V \delta\dot{\varepsilon}_{ij}\dot{\sigma}_{ij}\mathrm{d}V = -\int_V \delta\dot{\varepsilon}_{ij}\sigma^0_{ij}\mathrm{d}V. \tag{20}$$

where σ^0 and $\Phi^0(\overline{\sigma}(\overline{\varepsilon}^p), |\nabla\overline{\varepsilon}^p|, \nabla^2\overline{\varepsilon}^p)$ denote the solution of the previous incremental step. The equations above build the fundamentals for the finite element method. To solve the integral equations above a discretization method must be used to turn the partial differential equations to algebraic equations.

2.2 Finite element formulations

The element with the 8-nodal serendipity interpolation of displacement and 4-nodal Hermitian interpolation of equivalent plastic strain with 2×2 Gaussian point integration is the most reliable C^1-continuous element, as reported by Pamin (1994). Mikkelsen (1997) extended this element type to finite strain states and simulated necking of uniaxial tension test of ductile metallic materials. Due to the explicit Hermitian shape function which is introduced to satisfy requirements of the C^1 continuity, the element is constrained to be rectangular. Ramswamy and Aravas (1998) introduced the C^0 element by using the Gauss theorem in integration. Such formulation assumes a vanishing normal derivative of the equivalent plastic strain at all boundaries, $\partial\dot{\lambda}/\partial\mathbf{v} = 0$. The C^0 element formulation is attractive for general robust finite element computations, however, useful only for a model linearly depending on the equivalent plastic strain gradient as in equation (12). As soon as the gradient terms appear in a nonlinear form in the constitutive equation, as suggested by Nix and Gao (1998), the C^0 formulation becomes not applicable.

In this paper, we use the C^1-continuous finite element formulation in which the implicit Hermite interpolation functions suggested by Petera and Pittman (1994) are used for interpolating the equivalent plastic strain. The element can be transformed to an arbitrary quadrilateral form. Our computational analysis of the shear band support that such interpolation gives numerically reliable results [Chen, Yuan (2000)]. More recently, an alternative numerical method based on the meshless local Petrov-Galerkin technique is attractive [Atluri, Shen (2002); Kim, Atluri (2000)], which easily leads to C^1 type of interpolations in the local coordinate system. This is beyond the scope of the present paper. The reader who is interested in this topic is referred to the recent papers by Atluri and his co-workers [Atluri, Shen (2002); Kim, Atluri (2000)].

Using the two governing equations (19) and (20), we have two kinds of node degrees of freedom, i.e. the dis-

placement $\mathbf{u}$ and the equivalent plastic strain measure $\bar{\varepsilon}^p$. They are interpolated as

$$\mathbf{u}(\mathbf{x}) = [\mathbf{N}(\mathbf{x})]\mathbf{u}_{node}, \tag{21}$$

$$\bar{\varepsilon}^p(\mathbf{x}) = \lambda = [\mathbf{H}(\mathbf{x})]\mathbf{\Lambda}_{node}, \tag{22}$$

where $[\mathbf{N}(\mathbf{x})]$ is the standard 8-nodal serendipity interpolation function vector for displacement and $[\mathbf{H}(\mathbf{x})]$ is the C^1-continuous implicit Hermitian interpolation function vector for equivalent plastic strain. For details of such interpolation the reader is referred to the work of Petera and Pittman (1994). The two governing equations (19) and (20) can be re-written as

$$\int_v [\mathbf{B}]^T \dot{\boldsymbol{\sigma}} \mathrm{d}v = -\int_v [\mathbf{B}]^T \boldsymbol{\sigma}^{\mathbf{0}} \mathrm{d}v \tag{23}$$

$$\int_{v^p} [\mathbf{H}]^T (\mathbf{n}^T \dot{\boldsymbol{\sigma}} + \frac{\partial \Phi}{\partial \lambda}\dot{\lambda} + \frac{\partial \Phi}{\partial |\nabla\lambda|}|\nabla\dot{\lambda}| + \frac{\partial \Phi}{\partial \nabla^2 \lambda}\nabla^2\dot{\lambda})\mathrm{d}v$$

$$= -\int_{v^p} [\mathbf{H}^T]\Phi^0 \mathrm{d}V \tag{24}$$

In the incremental finite element algorithm, one must get the consistent tangent stiffness matrix for every increment to achieve a quadratic convergence rate of Newton's iteration algorithm. So the variation of stress status at the end of one increment is defined by the backward Euler integration algorithm,

$$\dot{\sigma}_{ij} = C_{ijkl}\dot{\varepsilon}_{kl} - C_{ijkl}n_{ij}\dot{\varepsilon}^p + \sigma_{ik}\Omega_{kj} - \sigma_{jk}\Omega_{ki}, \tag{25}$$

where $C_{ijkl} = [(C^e_{ijkl})^{-1} + \Delta\lambda\partial\Phi^2/\partial\sigma^2_{ij}]^{-1}$ and $\Delta\lambda$ is the increment of effective plastic strain in current incremental step. Substituting Equation (25) and expressions of $\partial\Phi/\partial\lambda$, $\partial\Phi/\partial|\nabla\lambda|$ and $\partial\Phi/\partial\nabla^2\lambda$ into the equations above, we can get the final equations of the finite element computations [Chen, Yuan (2000)].

3 Modeling

To simplify computational modeling the indenter is assumed to be axisymmetric conical. The half angle of the axisymmetric indenter is taken to be 72°, which corresponds to Berkovich indenter (Fig. 1). This assumption has been adopted by many previous micro-indentation simulations based on different gradient plasticity models [Begley, Hutchinson (1998); Nix, Gao (1998); Yuan, Chen (2001)]. 3D effects to such simplifications have been discussed in [Larsson, et al. (1996)]. The contact radius is defined as a and the depth of penetration of the indenter is δ. The indenter is assumed to be rigid. The contact between the indenter and the substrate is postulated frictionless.

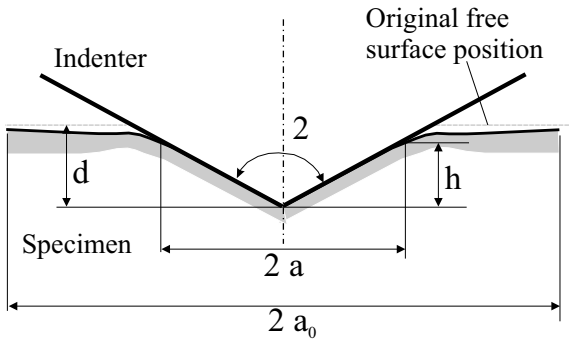

Figure 1 : Axisymmetric micro-indentation model used in the present computations. β denotes the half angle of indenter, h is the indentation depth and δ the displacement of indenter, a the radius of the contact area of the indentation, a_0 a global measurement of the specimen.

To make use of the contact element technique in ABAQUS and to visualize the finite element results using ABAQUS we embed an additional sheet of conventional isoparametric elements on the user element mesh with vanishingly small strength. It makes also possible to evaluate the reaction forces and strain distributions in the specimen.

The contact radius of indentation, a, can be determined by the vanishing contact force computed by ABAQUS. Due to the scattering of the a value proportional to the element size near the indenter tip, the final radius value must be smoothed. As soon as a is known, the indentation depth is calculated as

$$h = \frac{a}{\tan\beta}. \tag{26}$$

The force applied on the indenter, P, is used to compute the hardness as:

$$H = \frac{P}{\pi a^2}. \tag{27}$$

This method can be taken for all possible indenter angles and different indentation depths.

To non-dimensionalize computations we introduce the remote radius a_0. a_0 should be large enough in comparing with a to obtain the macro hardness value. When the mesh used for computations is fine enough, the final conclusions are independent of a_0.

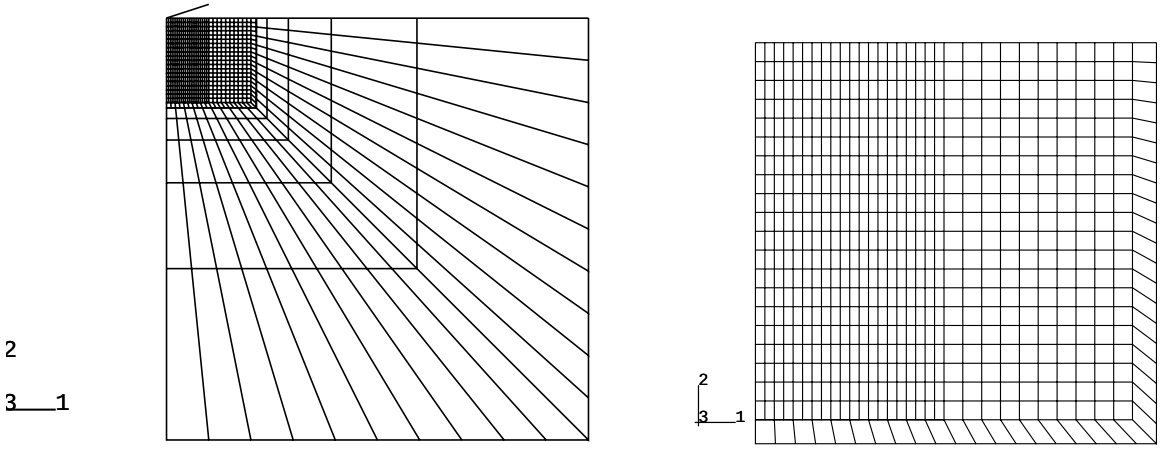

Figure 2 : A typical finite element mesh with C^1 continuity, with 650 elements and 3700 nodes, used for computations. All elements have 8 nodes for interpolation of displacement and 4 additional nodes for the effective plastic strain. The indenter is simulated with a rigid surface. (a) The full mesh. (b) The elements near to the indenter tip.

In this paper different finite element meshes are used to study the mesh-(in)dependence. It is confirmed that computational results under finite strain assumption are numerically mesh-insensitive when the contact surface is discretised by more than 10 elements. The scattering due to the discrete element size is limited to 5 % for performed computations. In this paper we just report numerical results with a kernel mesh 30×20 8-nodal elements with 4 node for interpolation of effective equivalent plastic strain near to the indenter tip. It means that only in this kernel mesh the gradient plasticity theory is applied. The conventional 8-nodal displacement element is used in the outer mesh due to the small plastic strain and its gradients. The mesh is shown in Fig. 2. In computations the absolute element size near the indenter tip varies with the given intrinsic material length scale proportionally. The final computational step just reaches half of the kernel. The whole mesh has a size as large as ten times the size of the kernel and the overall mesh size is defined as a_0 in our computations.

In most computational work on gradient plasticity published by de Borst and co-workers [deBorst, Mühlhaus (1992); Pamin (1994)], only the Laplacian of equivalent plastic strain was introduced into the constitutive relationship and flow stress, namely $\sigma_y = \overline{\sigma}(\overline{\varepsilon}^p) - g_2 \nabla^2 \overline{\varepsilon}^p$. In the analysis of strain-softening, Pamin (1994) suggested the gradient parameter $f_2 = -\overline{\sigma}'(\overline{\varepsilon}^p)$, where $-\overline{\sigma}'(\overline{\varepsilon})$ is the slope of the stress-strain curve measured in uniaxial tests. Such assumption makes a smooth increase and decrease of the gradients of plastic strain in computations. It is specially of importance as soon as the strains are localized increasingly. Ramaswamy (1998), Sverberg and Runesson (1998) and Mikkelsen (1997) use $f_2 = 1$ as constant in the shear band analysis for strain-hardening material. As stated by Pamin (1994), in the shear band, where intensive shearing occurs, $\nabla^2 \overline{\varepsilon}^p$ is negative, thus the gradient term will arise the flow stress there, while $\nabla^2 \overline{\varepsilon}^p$ becomes positive near the elastic-plastic boundary, which makes it possible for the localization zone to spread out the plastic zone due to the decrease of the flow stress. Furthermore, from torsion solutions one may conduct that the parameter g_2 must be a function of the plastic strain to avoid singular strain distribution.

In the numerical analysis of micro-indentation, we found in the area near the indenter tip, the Laplacian of the equivalent plastic strain oscillated strongly and were over hundreds times of the strain itself. Similar phenomena can be found in crack tip field analysis of ductile material. It implies that using constant parameter g_2 makes numerical computations difficult.

Generally we assume that, when the equivalent plastic strain is small, the influence of $\nabla^2 \overline{\varepsilon}^p$ should not be very strong on the strength of material in the area near the indenter tip. For large plastic strain the amplitude of g_2 should be limited and positive, i.e.

$$f_2(\overline{\varepsilon}^p) = \begin{cases} \left(\dfrac{\overline{\varepsilon}^p}{\overline{\varepsilon}_0^p}\right)^n & \text{if } \overline{\varepsilon}^p \le \overline{\varepsilon}_0^p \\ 1 & \text{if } \overline{\varepsilon}^p > \overline{\varepsilon}_0^p \end{cases} \tag{28}$$

Above we introduce two parameters, the exponent n and the range $\overline{\varepsilon}_0^p$. Computations with $1 < n < 3$ show a stable numerical convergence. The final computational results are very slightly affected by n and $\overline{\varepsilon}_0^p$ values. In computations reported in the present paper we set $n = 2$ and $\overline{\varepsilon}_0^p = 0.1$. This assumption will not change our conclusions.

4 Results and discussions

The initial input data adopted in the present computations are taken from the paper of Begley and Hutchinson (1998), with plastic strain hardening exponents $N = 1/3$, $N = 1/5$ and $N = 1/10$. Furthermore, we assume Young's modulus $E = 300\sigma_0$ and Poisson's ratio $\nu = 0.3$. For these parameters the finite element computations predict macro-hardness of $H_0 = 7.89\sigma_0$, $5.28\sigma_0$ and $3.89\sigma_0$ for $N = 1/3$, $1/5$ and $1/10$, respectively, under finite strain and plastic flow theory assumptions. These predictions agree with the results of Begley and Hutchinson (1998).

It is worth noticing that to avoid artificial effects in numerical fitting, we did not take any additional fitting algorithm in hardness evaluation. The scattering of the data is caused by finite element discretization. The contact area is directly evaluated from the contact elements and, therefore, spreads discontinuously. This scattering grows with the strain exponent N. For materials with higher plastic strain hardening, the scattering is larger.

4.1 The role of the second-order derivative (Laplacian) of plastic strain

In this subsection we assume $c_1 = 0$ and study the effect of the second-order derivative (Laplacian) of equivalent plastic strain, c_2, only. The assumption in (28) is introduced. The micro-hardness H over macro-hardness H_0 is plotted as a function of indentation depth h in Fig. 3. In the figures the symbols denote the computational results and the solid lines are fitted according to a suggestion of Nix and Gao (1998). Variations about c_2 are shown for $N = 1/10$ in Fig. 3(a). The gradient regulator c_2 increases the strength of the continuum model and so the hardness. For the same macro-hardness, the micro-hardness for small h from the finite element computations is significantly larger than Nix and Gao prediction.

In Fig. 3(b) the depth is normalized by the intrinsic material length c_2. This figure verifies that the micro-hardness explicitly depends on h/c_2, i.e. $H = H_0\psi(h/c_2)$. The influence of the parameter c_2 can be scaled if the horizontal axis is normalized by c_2.

From Nix and Gao (1998) we know H^2 is a linear function of $1/h$. In Fig. 4 the normalized hardness is plotted as function of c_2/h. Figure 4(a) shows that the correlation between H^2 and $1/h$ is nonlinear. The solid lines are a least square fitting of the computational results. The Aifantis' model with Laplacian gradient regulator provides a significant overestimate in comparison with experimental fitting for some metals in [Nix, Gao (1998)].

It is interesting to find from Fig.4(b) that the present results are similar to those obtained using Fleck-Hutchinson strain gradient plasticity model in Begley and Hutchinson (1998). The computational prediction of micro-hardness is approximated by a linear function, that is,

$$\frac{H}{H_0} = 1 + c^* \left(n, \frac{\sigma_0}{E}\right) \frac{c_2}{h},$$

where $c^*(n, \sigma_0/E)$ is a coefficient depending on mechanical property of materials. For the present computations the linear fitting is valid only for $c_2/h \geq 1$.

4.2 The role of the first-order derivative of plastic strain

In discussion of the last section the gradient regulator is related with the second gradient of the plastic strain. It is not suitable for simple bending tests in which the strain is distributed linearly. In the four-point-bending experiment of mild steel beams, Richard (1958) observed the size effect of yield initiation (upper yield stress) and interpreted it using statistical model. To catch this effect one must include the first order of plastic strain gradient into the constitutive model.

We set $f_1(\overline{\varepsilon}^p) = 1$ in Equation (10) and $g_2 = 0$. The flow stress is defined as $\sigma_y = \overline{\sigma}(\overline{\varepsilon}^p) + \sigma_0 c_1 |\nabla \overline{\varepsilon}^p|$. Due to the positive value of $\nabla \overline{\varepsilon}^p$, the strength of material is 'hardened' when the strain gradient exists.

Micro-hardening from finite element computations, H, is shown in Fig. 5 as a function of the indentation depth h. The diagrams are non-dimensionalized by the macro-hardness H_0 and by a_0 or c_1, respectively. The symbols are finite element computations and the solid lines are predictions of Nix and Gao (1998). Significant increase of micro-hardness is restricted near $h \to 0$. As in Yuan, Chen (2001) variations about the intrinsic material length

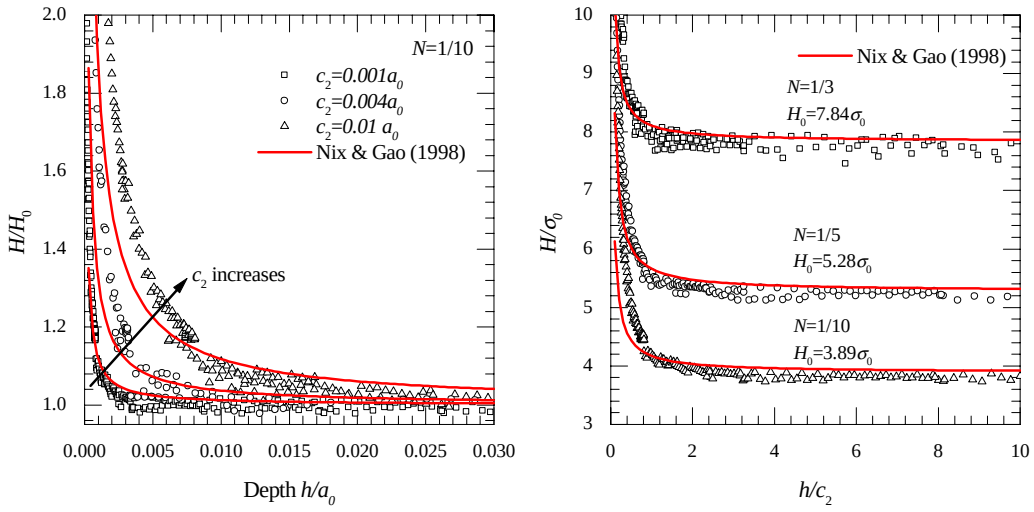

Figure 3 : Depth-dependence of the micro-hardness. The symbols stand for computational finite element results. Lines are predictions of Nix and Gao (1998). Only the Laplacian of plastic strain is considered into the formulation of the flow stress ($c_1 = 0$). (a) Effects of intrinsic material length c_2. (b) Effects of strain hardening exponent N.

in Fig. 5(a) can be scaled by the material length, as plotted in Fig. 5(b).

The present computational results using the first order gradient of equivalent plastic strain agree reasonably with the prediction of Nix and Gao (1998), as shown in Fig. 5(a). A plot of $(H/H_0)^2$ over c_1/h of Fig. 6 confirms, furthermore, that this agreement is limited to $c_1/h \leq 6$. Beyond this region the finite element computation under-estimates the micro-hardness, in comparison with Nix and Gao (1998). This has been reported in an other systematic study of micro-hardness simulation using a different flow stress equation [Yuan, Chen (2001)]. It is reasonable that as the depth h decreases, the micro-hardness cannot increase to infinity, as $h \to 0$, and should have a maximum value depending on material length scales, that means, the linear relations between H/H_0 and $1/h$ should be satisfied only in an appropriate range. Then gradient plasticity theory, using the first-order derivative only in the constitutive formulation can give a reasonable approximation for small c_1/h to the prediction of Nix and Gao (1998).

It is interesting to see that in the micro-indentation simulations, the first-order derivative of equivalent plastic strain, $|\nabla\bar{\varepsilon}^p|$, is more suitable to model the known hardness variations than the Laplacian of plastic strain, $\nabla^2\bar{\varepsilon}^p$, whereas in shear band analysis, only $\nabla^2\bar{\varepsilon}^p$ can prevent strain localizations.

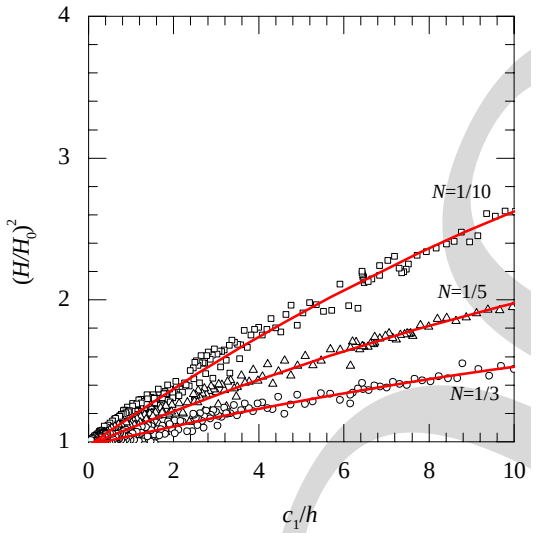

Figure 6 : Micro-hardness as a function of the inverse of indentation depth. The symbols stand for computational finite element results. The solid lines denote the least square fitting using a square function. Only the first-order derivative of plastic strain, $|\nabla\bar{\varepsilon}^p|$, is included in the constitutive equations ($c_2 = 0$).

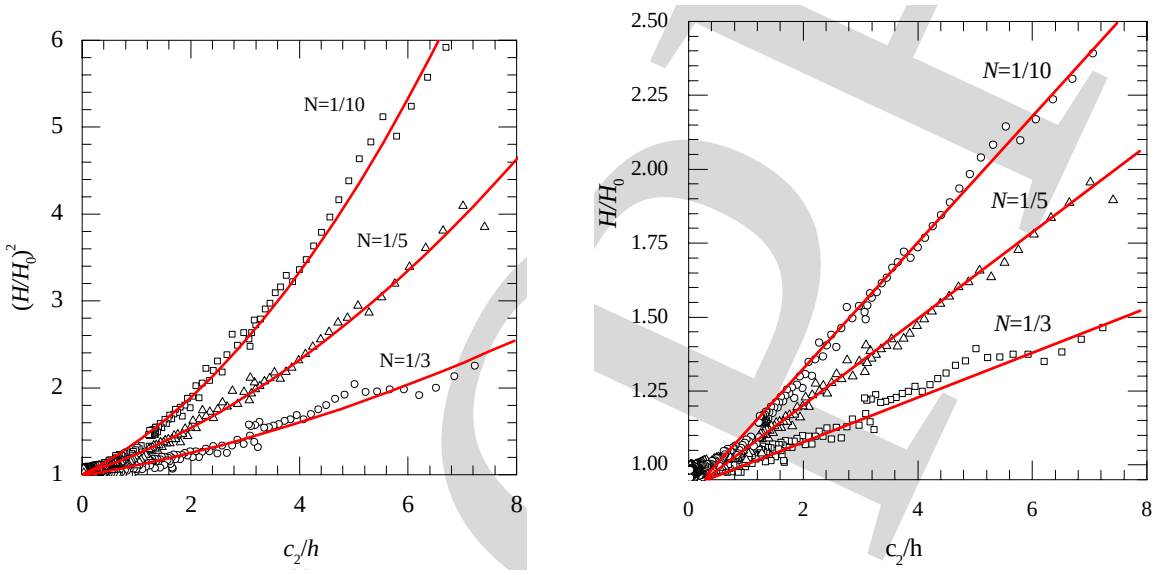

Figure 4 : Micro-hardness as a function of the inverse of indentation depth. The symbols are computational results with $N = 1/10$, $/5$ and $1/3$, respectively. The solid lines are the least square fitting using a square function. Only the Laplacian of plastic strain is considered into the formulation of the flow stress. (a) A square plot. (b) A linear plot.

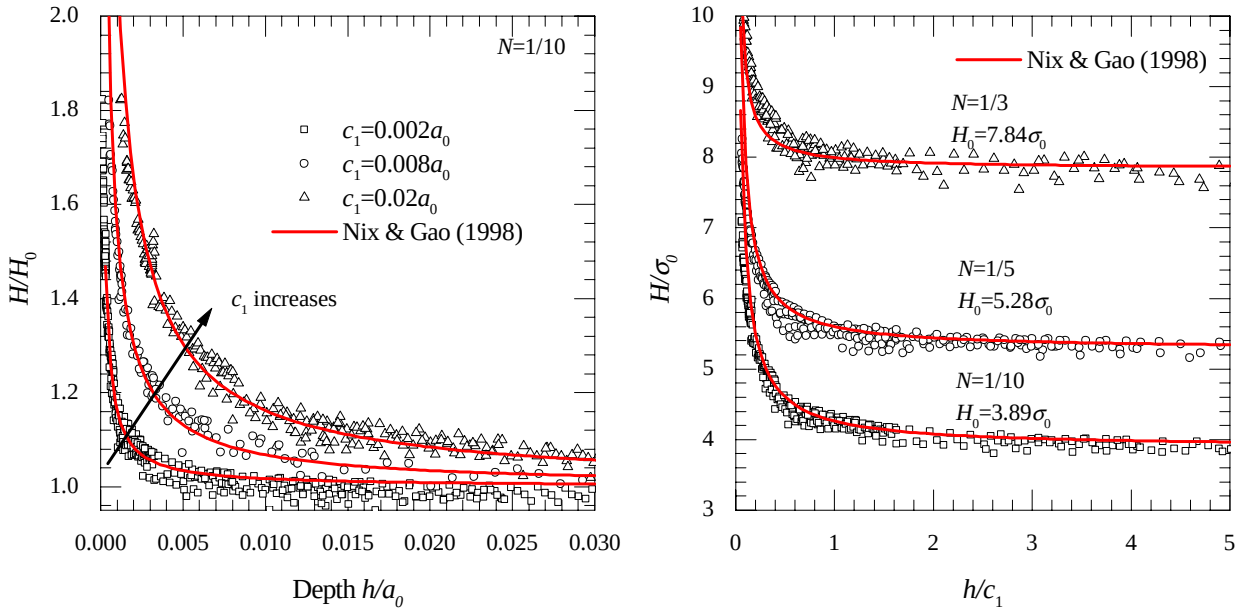

Figure 5 : Depth-dependence of the micro-hardness. The symbols stand for computational finite element results. The solid lines are predictions of Nix and Gao (1998). Only the first-order derivative of plastic strain, $|\nabla\bar{\varepsilon}^p|$, is included in the constitutive equations ($c_2 = 0$). (a) Effects of intrinsic material length c_1. (b) Effects of strain hardening exponent N.

4.3 The role of the two material length scales

From the discussions above one can see the model with the Laplacian of plastic strain may only give a strong effect on micro-hardness variations, while the first gradient of equivalent plastic strain leads to moderate increase of the predicted hardness. To fit different hardness variations in different materials, one may adjust both material length parameters. From this point of view, both parameters have to be determined by experimental data.

In Fig. 7(a) three curves are depicted with different c_1 and c_2 for $N = 1/10$. This figure indicates that to fit the linear relationship, the length scale c_2 is far smaller than the length scale c_1 since $\nabla^2\bar{\varepsilon}^p$ has a much stronger effect on the increase of micro-hardness. In Fig. 7(b) the data are depicted with different c_2 and constant c_1 for the same plastic strain exponent. It shows that using different values of length scale c_2, the effect of $\nabla^2\bar{\varepsilon}^p$ increases or decreases strongly and the micro-hardness deviates gradually from the linear relation. From these figures and the numerical calculation we find when $c_1 = 3c_2 \sim 8c_2$ the computational results do produce the linear relation between H/H_0 and $1/h$ over the whole computational range.

5 Conclusions

In the present paper we discussed simulations of micro-indentation tests using Aifantis' gradient plasticity model. Both gradient terms of equivalent plastic strain in the gradient plasticity model are considered.

Computations confirm that the micro-hardness predicted by the gradient plasticity varies with indentation depth, as soon as the gradient regulators differ from zero. Depth-dependence of micro-hardness can be simulated using gradient plasticity models.

Variations of micro-hardness is correlated with the intrinsic material length parameters. In comparison with experimental results of Nix and Gao (1998), the Aifantis' model using the Laplacian term of equivalent plastic strain provides an overestimate, whereas the first gradient term under-estimates the hardness variations.

Based on extensive computations one can figure out a correlation between the intrinsic material length, mechanical property and micro-hardness, as discussed in Yuan, Chen (2001). Micro-hardness tests provide a method to determine the intrinsic material length in the gradient plasticity models.

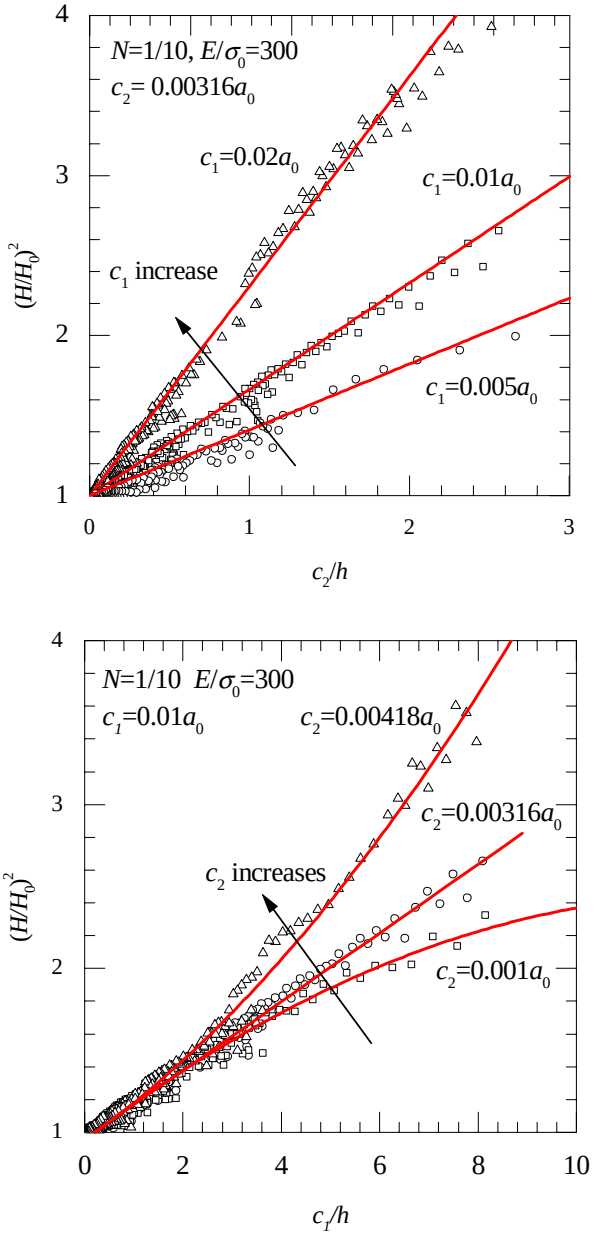

Figure 7 : Interaction of both intrinsic material length parameters. The symbols stand for computational finite element results. The solid lines denote the least square fitting using a square function. (a) $c_2 = 0.00316a_0$. (b) $c_1 = 0.01a_0$.

Reference

ABAQUS User Manual, Version 5.6, Hibbitt, Karlsson and Sorensen, Inc., Providence, R. I. (1996).

Aifantis, E. C. (1987). The physics of plastic deformation. *International Journal of Plasticity*, **3**, pp. 211-247.

Aifantis, E. C. (1999). Strain gradient interpretation of size effects. *International Journal of Fracture*,**93**, pp. 299-314.

Atluri, S.N. (1984). On constitutive relations at finite strain: hypo-elasticity and elasto-plasticity with isotropic or kinematic hardening. *Computer Methods in Applied Mechanics and Engineering*, **43**, pp. 137-171.

Atluri, S.N. and Shen, S (2002). The Meshless Local Petrov-Galerkin (MLPG) Method: A simple and less-costly alternative to the finite element and boundary element methods. *Computer Modeling in Engineering & Sciences*, **3**, pp. 1-40.

Begley, M., Hutchinson, J.W (1998). The mechanics of size-dependent indentation. *Journal of Mechanics and Physics of solids*, **46** pp. 2049-2068

Chen, J. and Yuan, H. (2000). A micromechanical damage model based on gradient plasticity: Algorithms and applications. *International Journal for Numerical Methods in Engineering*, **54**, pp. 399-420.

de Borst, R., and Mühlhaus, H. (1992). Gradient-dependent plasticity: formulation and algorithmic aspects. *International Journal for Numerical Methods in Engineering*, **35**, pp. 521-539.

de Guzman, M. S., Neubauer,G., Flinn, P. and Nix, W.D. (1993). The role of indentation depth on the measured hardness of materials. *Mater. Res. Symp. Proc.*, **308**, pp. 613-618.

Fleck, N. A., and Hutchinson, J. W. (1993). A phenomenological theory for strain gradient effects in plasticity. *Journal of the Mechanics and Physics of Solids*, **41**, pp. 1825-1857.

Fleck, N. A., and Hutchinson, J. W. (1997). Strain gradient plasticity. *Advances in Applied Mechanics*, **33**, pp. 295-361.

Gao, H., Huang, Y., Nix, W. D., and Hutchinson, J. W (1999). Mchanisms-based strain gradient plasticity-theory and experiment. *Journal of the Mechanics and Physics of Solids*, **47**, pp. 1239-1293.

Huang, Y., Gao, H., Nix, W. D., and Hutchinson, J. W (2000). Mchanisms-based strain gradient plasticity-II. *Journal of the Mechanics and Physics of Solids*, **48**, pp. 99-128.

Kim, H. G. and Atluri, S. N. (2000). Arbitrary placement of secondary nodes, and error control, in the meshless local Petroc-Galerkin (MLPG) method. *Computer Modeling in Engineering & Sciences*, **1**, pp. 11-32.

Larsson, P.-L., Giannakopoulos, A.E., Sunderland, E., Rowcliffe, D.J., and Vestergaard, R. (1996). Analysis of Berkovich indetation. *International Journal of Solids and Structures*, **33**, pp. 221-248.

Ma, Q. and Clarke, D. R (1995). Size dependent hardness in silver single crystals. *Journal of Materials Research*, **10**, pp. 261-278.

McEkhaney, K. W, Vlassak, J. J and Nix, W.D. (1998). Determination of indenter tip geometry and indentation contact area for depth-sensing indentation experiments. *Journal of Materials Research*, **13**, pp. 1300-1306.

Mikkelsen, L. P. (1997). Post-necking behaviour modelled by a gradient plasticity theory. *International Journal of Solids and Structures*, **34**, pp. 4531-4546.

Mühlhaus, H. B., and Aifantis, E. C. (1991). A variational principle for gradient plasticity. *International Journal of Solids and Structures*, **28**, pp. 845-857.

Nix, W. D. and Gao, H. (1998). Indentation size effects in crystallie materials, A law for strain gradient plasticity. *Journal of the Mechanics and Physics of Solids*, **46**, pp. 411-425.

Pamin, J. (1994). Gradient-dependent plasticity in numerical simulation of localization phenomena. PhD-Thesis, Delft University of Technology, Netherlans, 1994, pp. 3489-3519.

Petera, J., and Pittman, J. F. T. (1994). Isoparametric Hermite elements. *International Journal for Numerical Methods in Engineering*, **37**, pp. 3489-3519.

Polizzotto, C. and Borino, G. (1998). A thermodynamics-based formulation of gradient-dependent plasticity. *Europe Journal of Mechanics A/Solids*, **17**, pp. 741-761.

Poole, W.J., Ashby, M.F. and Fleck, N.A. (1996) Micro-hardness tests on annealed and work-hardened copper polycrystals. *Scripta Metall. Mater.*, **34**, pp. 559-564.

Ramaswamy, S. and Aravas, N. (1998). Finite element implementation of gradient plasticity models, Part I, Part

II. *Computer Methods in Applied Mechanics and Engineering*, **163** pp.11-32, pp. 33-53.

Richard, C. W. (1958). Effect of size on the yielding of mild steel beams. *Proc. Am. Soc. Testing Mater.*, **58** pp. 955-970.

Stelmashenko, N. A., Walls,M.G., Brown, L.M. and Miman,Y.V. (1993). Microindentation on W and Mo oriented single crystals: An SEM study. *Acta Metallica Materiala*, **41** pp. 2855-2865.

Shu, J. Y. and Fleck, N. A. (1998). The prediction of a size effect in micro indentation. *International Journal of Solids and Structures*, **161** pp. 49-65.

Sverberg, T., and Runesson, K. (1998). An algorithm for gradient-regularized plasticity coupled to damage based on a dual mixed FE-formulation. *Computer Methods in Applied Mechanics and Engineering*, **161** pp. 49-65.

Valanis, K. C. (1997). A gradient theory of finite viscoplasticity. *Arch. Mech.*, **49** pp. 589-609.

Yuan, H. and Chen, J. (2000). Analysis of size effects based on a lower-order gradient plasticity model. *Computational Material Science*, **19**, pp. 143-157.

Yuan, H., and Chen, J. (2001). Identification of intrinsic material length in gradient plasticity from microindentations. *International Journal of Solids and Structures*, **38**, pp. 8171-8187.

Zienkiewicz, O.C. (1971). The finite element method in engineering science. MacGraw-Hill Publ. Comp., London.